Data-Driven Phase-Based Control of a Powered Knee-Ankle Prosthesis for Variable-Incline Stair Ascent and Descent

Ross J. Cortino, T. Kevin Best, and Robert D. Gregg

Abstract—Powered knee-ankle prostheses can offer benefits over conventional passive devices during stair locomotion by providing biomimetic net-positive work and active control of joint angles. However, many modern control approaches for stair ascent and descent are often limited by time-consuming handtuning of user/task-specific parameters, predefined trajectories that remove user volition, or heuristic approaches that cannot be applied to both stair ascent and descent. This work presents a phase-based hybrid kinematic and impedance controller (HKIC) that allows for semi-volitional, biomimetic stair ascent and descent at a variety of step heights. We define a unified phase variable for both stair ascent and descent that utilizes lowerlimb geometry to adjust to different users and step heights. We extend our prior data-driven impedance model for variableincline walking, modifying the cost function and constraints to create a continuously-varying impedance parameter model for stair ascent and descent over a continuum of step heights. Experiments with above-knee amputee participants (N=2) validate that our HKIC controller produces biomimetic ascent and descent joint kinematics, kinetics, and work across four step height configurations. We also show improved kinematic performance with our HKIC controller in comparison to a passive microprocessor-controlled device during stair locomotion.

I. INTRODUCTION

Conventional passive knee-ankle prostheses are unable to provide the net-positive work at the joints needed for normative stair ascent and other activities of daily living [1]. Despite this lack of energy input, people with above-knee amputation (AKA) can still perform these activities but must rely on compensatory behaviors such as hip hiking [2]. Most prosthesis users are limited to performing step-to stair ascent, which halves the rate at which users can progress up a staircase. Step-to ascent is characterized by a person climbing only one stairstep per gait cycle, instead of two stairsteps as seen in step-over stair ascent. These compensatory behaviors, along with the lack of net-positive work from the passive device, often put extra strain on individual's sound leg and upper body [3]–[5] and can lead to secondary conditions such as chronic back pain and arthritis in the sound leg [6]–[8].

Able-bodied (AB) stair descent is characterized by a toestrike and the dissipation of energy by the ankle at the beginning of the gait cycle [1]. Passive devices are unable to reach this configuration, due to a lack of controlled plantarflexion at the ankle [9], resulting in a heelstrike (HS) at

This work was supported by the National Institute of Child Health & Human Development of the NIH under Award Number R01HD094772 and by the National Science Foundation under Award Number 2024237 and DGE 1841052. The content is solely the responsibility of the authors and does not necessarily represent the official views of the NIH or NSF.

R. J. Cortino, T. K. Best, and R. D. Gregg are with the Department of Robotics, University of Michigan, Ann Arbor, MI 48109. Contact: {cortinrj tkbest, rdgregg}@umich.edu

the beginning of the stance phase. To compensate for this behavior, amputee users must HS at the edge of the step, using that edge as a pivot for the foot to achieve the necessary flexion at the knee [9]. This inability to actively control joint angles affects both ascent and descent, leading to potential toe-stubbing during swing and loss of balance.

Emerging powered prosthetic devices [10]–[16] can address these challenges by contributing net-positive work during stair ascent, controlled negative work during stair descent, and active control of foot placement during both activities. Studies have also shown that powered devices can reduce joint power and strain on the contralateral side and limit hip compensation during stair locomotion [17], [18]. Despite the potential benefits of using powered devices, designing control approaches that can accommodate the various activities and environments of day-to-day life is still a challenge.

Traditionally, powered prostheses have been controlled to emulate human joint impedances at discrete phases of gait with a finite-state machine (FSM) [19]. These simple-to-implement impedance controllers have demonstrated promising results for level-ground walking, ramp ascent and descent, and stair ascent and descent [17], [18], [20]–[24]. The standard impedance controller parameterizes torque, τ , as a function of joint angle θ and velocity $\dot{\theta}$ in the form of

$$\tau = -K(\theta - \theta_{eq}) - B\dot{\theta},\tag{1}$$

where K, B, and $\theta_{\rm eq}$ are impedance parameters defining a joint's stiffness, damping, and equilibrium angle, respectively. Typically, the gait cycle is divided into 3-4 phases, each with a unique set of constant impedance parameters.

A major drawback of traditional FSM impedance control is that researchers must experimentally tune the impedance parameters for each discrete phase within the gait cycle. Similarly, thresholds based on sensor readings (foot contact (FC), joint kinematics, elapsed time, etc.) that control the switching between FSM phases must also be tuned. These tuneable parameters are often user/task-specific [21]. For example, Lawson et. al. proposed an FSM impedance controller for stair locomotion that had a combination of approximately 40 tuneable parameters and state switching criteria [20]. Moreover, staircases can vary greatly in incline or step height (even ADA-regulated staircases), and able-bodied studies have shown corresponding variations in normative joint kinetics and kinematics [1], [18], [25]-[27]. Therefore, the necessary impedance parameters and switching criteria also need to vary as a function of stair configuration, but the resulting tuning sessions would be infeasible in duration. Failure to adapt to variations in step height/inclination would likely result in improper biomechanics and issues with foot placement, compromising the performance of powered devices.

1

Rather than using heuristic strategies to reduce the number of tuned impedance parameters [21] or automating the tuning process for a limited set of parameters [28]–[30], our research group previously aimed to avoid parameter tuning altogether by using data-driven models based on pre-recorded AB kinematics [31]–[35]. In our recent stair ascent controller [35], AB joint kinematics parameterized by a thigh-based phase variable gave the user indirect-volitional control over the gait cycle progression and produced appropriate kinematics at the knee and ankle joints. However, this kinematic control method proved to be problematic when applied to stair descent (in preliminary work) due to this activity's small hip range of motion (ROM). In particular, small changes in thigh angle map to large changes in the phase variable and therefore in the desired knee and ankle angles. This sensitivity between the user's hip input and the resulting prosthesis joint patterns can cause swing phase oscillations or overly-aggressive gait progression. Therefore, an alternative approach for stair descent is needed.

To remedy the issues with purely kinematic control, Best et al. proposed a hybrid kinematic impedance controller (HKIC) for variable-speed/incline walking [36]. While the swing period was largely unchanged from previous kinematic methods, the controller continuously varied stance-phase joint impedance based on phase and task variables to produce biomimetic joint kinetics and work trends as task varied. These joint impedance models were generated through optimization with able-bodied kinematic/kinetic data. Another study applied this impedance control framework to sitting and standing and demonstrated similarly promising results [37].

Therefore, this work extends the HKIC approach by creating a continuously-varying impedance model for use in the stance phase of stair ascent and descent. Because impedance control regulates the relationship between joint angle and torque rather than controlling the joint angle directly, this HKIC approach remedies the aforementioned problems with a purely kinematic approach. This work's novel contributions include an adaptation of the impedance optimization problem originally outlined in [36] to calculate stair ascent/descent impedance parameters over a continuum of step heights. The cost function and constraints were modified to emphasize late-stance knee damping in stair descent, allowing the use of a thigh-based phase variable with a small thigh ROM. We also define a common phase variable for both stair ascent and descent that uses leg geometry to automate the user/task-specific parameter tuning needed to obtain linear phase estimates. Finally, we show that the HKIC controller produces biologically similar ascent/descent joint kinematics, kinetics, and work across four step height configurations during experiments with two AKA participants.

II. RELATED STAIR CONTROLLERS

Many researchers have suggested approaches to remedy the tuning burden, focusing on parameter reduction, automated parameter tuning, or both. Groups have applied fuzzy logic or reinforcement learning (RL) to automatically tune impedance parameters, offline or online, at the knee joint while users

walk [29], [30], but these approaches have not been applied to dual joints nor stair ascent/descent. Simon et al. reduced the number of tuneable parameters in a multi-activity controller from 140 to 20 by constructing mathematical relationships between parameters [21]. However, many of the parameters for stair locomotion were still hand-tuned, contributing to lengthy tuning sessions of about 5 hours for multiple activities. Other groups reduced the number of tuneable parameters by utilizing time-based, predefined joint torque trajectories during certain states within the stair ascent and descent gait cycles [22]. However, time-based trajectories can become desynchronized with the user, particularly during non-steady motions. Hybrid control approaches serve as another parameter reduction technique. One previous hybrid control approach for stair descent utilized traditional impedance control with constant sub-state parameters during stance and kinematic control during swing [11]. By utilizing kinematic control in swing, the number of tuneable impedance parameters was reduced by half. These hybrid approaches to control are similar to that proposed in this work but, to the authors' knowledge, no previous work with this architecture has utilized continuous, phase-based control for stair ascent and descent.

Other stair control methods give users indirect volitional control over the device by adapting joint kinematics and/or kinetics to user movement or intent. Hoover et al. utilized a traditional FSM fixed-impedance controller but modulated the provided knee torque during stance and terminal swing based on electromyography signals from the residual limb [38]. This approach to volitional control was limited to stair ascent and struggled during swing to achieve proper foot placement on the following stair step. Hood et al. presented a tuned-heuristic approach that, during swing, modulates the prosthetic joint angles based on the user's thigh angle, and during stance, modulates the knee joint torque-angle relationship based on the prosthesis knee position at FC [39]. While this approach allowed for adaptive stair ascent over two ADA-compliant stair configurations [40], the resulting kinetic and kinematic profiles were not evaluated for biomimicry, and the heuristic method was not applicable to stair descent.

III. CONTROL ARCHITECTURE FOR STAIR LOCOMOTION

Our proposed HKIC controller for variable-height stair ascent and descent builds upon our previous work on a purely kinematic controller for stair ascent [35], as well as our previous HKIC controller for variable-speed/incline walking [36]. During stance, the controller utilizes a joint impedance model that modulates stiffness, damping, and equilibrium angle as continuous functions of stance phase and step height (between 102 and 178 mm). In swing, the controller utilizes a kinematic controller that likewise modulates joint angles as functions of swing phase and step height, similar to [34], [35]. We also propose a modified phase variable that accounts for a user's specific leg geometry and better parameterizes the stance and swing phases.

A. Common Phase Estimate for Stair Ascent/Descent

We extend our previous phase estimation technique [35] through 1) independent calculation of stance phase variable

 $s_{\rm st}$ and swing phase variable $s_{\rm sw}$, and 2) the addition of a leg geometry-based optimization of phase variable parameters. These additions allow for a common phase-variable definition for all stair locomotion tasks and provide an automated way to individualize the phase variable for a user.

In our previous work [35], we proposed a phase variable defining the gait cycle between maximum hip flexion (MHF) events, instead of the traditional gait cycle defined by HS. However, MHF detection was unreliable and depended on participant-specific tuning of detection thresholds. To alleviate this issue, as well as bring the stairs phase variable into parity with other activities [36], [37], we propose a phase variable for both ascent and descent that defines the gait cycle by foot-strike (FS). We choose to use the term FS instead of the traditional HS due to initial FC in descent being characterized by a toestrike instead of the HS experienced in ascent. Further, we improve on previous phase variable definitions by decoupling the stance and swing portions of the gait cycle, defining them by a stance phase variable s_{st} and swing phase variable s_{sw} . This removes the interdependence of the kinematic and impedance control frameworks on each other, allowing for modifications of phase parameters for one sub-controller to have little to no effect on the behavior of the other. Our gait cycle phase variable s is thus defined as

$$s = s_{\text{st}} \cdot \hat{s}^{\text{TO}} + s_{\text{sw}} \cdot (1 - \hat{s}^{\text{TO}}), \tag{2}$$

where \hat{s}^{TO} is the average able-bodied value of normalized time at which TO occurs for each stair locomotion task.

An FSM governs changes between phase variable definitions at biologically-inspired thresholds, such as maximum hip extension (MHE) or toe-off (TO). Fig. S1 shows the state transition criteria, with states S1 through S3 corresponding to stance and states S4 and S5 corresponding to swing. The redundant state in stance, S2, acts as a threshold to prevent premature MHE detection (as described later). The feedforward state S5 is a notable addition to our state machine from our previous stair ascent controller [35].

1) Stance Phase Variable Definition: Our FSM begins in S1 after FS is detected. During S1, we define our stance phase estimate \hat{s}_{st} with the descending phase definition

$$\hat{s}_{\text{st}} = \frac{\theta_{\text{th}}^{\text{FS}} - \theta_{\text{th}}}{\theta_{\text{th}}^{\text{FS}} - \theta_{\text{th}}^{\text{MHE}}} \cdot s_{\text{st}}^{\text{MHE}} \quad \text{for S1 \& S2,}$$
 (3)

where parameters $\theta_{\rm th}^{\rm FS}$, $\theta_{\rm th}^{\rm MHE}$, and $s_{\rm st}^{\rm MHE}$ denote the estimated thigh angle at FS, thigh angle at MHE, and stance phase at MHE, respectively. This phase definition is valid until MHE, but we use this phase definition over two states S1 and S2 to prevent premature MHE detection that can occur with slow strides during thigh extension in S1. The FSM stays in S1 as thigh angle $\theta_{\rm th}$ decreases until a threshold $s_{1\to 2}=0.85 \cdot s_{\rm st}^{\rm MHE}$ is reached, corresponding to the stance phase at which we expect the thigh velocity to begin slowing. MHE detection is only done in S2, where we employ a fast (10 ms) and slow (40 ms) simple moving average minima detection algorithm on the measured thigh angle inspired by financial stock trend analysis techniques [41]. This approach filters out noise in the thigh angle measurement as the user approaches MHE to prevent premature detection.

After MHE occurs, the FSM transitions to S3 for the remainder of stance. During S3, we define our stance phase estimate with the ascending phase definition

$$\hat{s}_{\text{st}} = 1 + \frac{\theta_{\text{th}} - \theta_{\text{th}}^{\text{TO}}}{\theta_{\text{th}}^{\text{FS}} - \theta_{\text{th}}^{\text{m}}} \cdot (1 - s_{\text{st}}^{\text{m}}) \quad \text{for S3}, \tag{4}$$

where parameters $\theta_{\rm th}^{\rm TO}$, $\theta_{\rm th}^{\rm m}$, and $s_{\rm st}^{\rm m}$ denote the estimated thigh angle at TO, measured thigh angle at MHE, and measured stance phase at MHE, respectively. After the loss of FC, the stance phase estimate is saturated at $\hat{s}_{st}=1$ for the remainder of the gait cycle (during S4 and S5).

2) Swing Phase Variable Definition: Following TO, the FSM transitions from S3 to S4, where the ascending θ_{th} trajectory gives rise to our estimated swing phase variable

$$\hat{s}_{\text{sw}} = \frac{\theta_{\text{th}} - \tilde{\theta}_{\text{th}}^{\text{TO}}}{\tilde{\theta}_{\text{th}}^{\text{MHF}} - \tilde{\theta}_{\text{th}}^{\text{TO}}} \cdot s_{\text{sw}}^{\text{MHF}} \quad \text{for S4}, \tag{5}$$

where $\tilde{\theta}_{\rm th}^{\rm TO}$ is the measured thigh angle at TO and $s_{\rm sw}^{\rm MHF}$ is the anticipated swing phase at which MHF occurs. We estimate $\theta_{\rm th}$ at MFH as $\tilde{\theta}_{\rm th}^{\rm MHF} = \max(\tilde{\theta}_{\rm th}^{\rm TO}, \theta_{\rm th}^{\rm TO}) - \theta_{\rm th}^{\rm TO} + \theta_{\rm th}^{\rm MHF}$, which enforces the minimum angular separation between $\tilde{\theta}_{\rm th}^{\rm TO}$ and $\tilde{\theta}_{\rm th}^{\rm MHF}$ shown in the training dataset for the given task. The FSM transitions from S4 to S5 at thigh velocity of $\tilde{\theta}_{\rm th} \leq 0.75$ rad/s and $\theta_{\rm th}$ greater than or equal to $\theta_{\rm th}^{4\to5}$. The thigh angle threshold $\theta_{\rm th}^{4\to5} = \frac{1}{4}\tilde{\theta}_{\rm th}^{\rm TO} + \frac{3}{4}\tilde{\theta}_{\rm th}^{\rm MHF}$ corresponds to the end of the linear portion of thigh flexion. The thigh velocity threshold is chosen to prevent an early switch to S5 if the user has not yet left the linear portion of thigh flexion.

After transitioning from S4 to S5, a feed-forward phase definition based on the average swing phase rate in S4, \dot{s}_{sw}^4 , is used similarly to [36]:

$$\hat{s}_{\text{sw}} = \hat{s}_{\text{sw}}^{45} + \int_{0}^{\Delta t} \dot{s}_{\text{sw}}^{4} d\tau \quad \text{for S5},$$
 (6)

where \hat{s}_{sw}^{45} is the estimated swing phase when the FSM transitions from S4 to S5. This implementation of a feedforward phase rate prevents premature saturation of the phase variable, due to $\theta_{\rm th}^{\rm MHF}>\theta_{\rm th}^{\rm FS}$ for all stair locomotion tasks. Excessive phase saturation before MHF is undesirable because a phase variable with a non-unity slope will temporally scale the joint trajectories at the knee and ankle, desynchronizing the user and device. This can lead to tripping and loss of balance. If the user is ascending or descending consistently and thigh features are estimated correctly, $\hat{s}_{sw} = 1$ will occur simultaneously with FS, returning the FSM to S1. However, we allow saturation of \hat{s}_{sw} in S5 after MHF so the knee reaches the necessary flexion (ascent) or extension (descent) angles early enough that the user has confidence it is ready to accept their weight upon FS. In pilot testing, users noted their preference for this behavior to resemble their experience with conventional prostheses. At FS, the state machine transitions from S5 to S1 and the process repeats for the next stair stride. During the stance portion of the gait cycle, S1-S3, our swing phase estimate is fixed at $\hat{s}_{sw} = 0$.

3) Geometry-Based Thigh Feature Estimation: In order to calculate an accurate phase variable, correct estimation of the user's thigh trajectory features (θ_{th}^{FS} , θ_{th}^{MHE} , θ_{th}^{TO} , θ_{th}^{MHF}) is

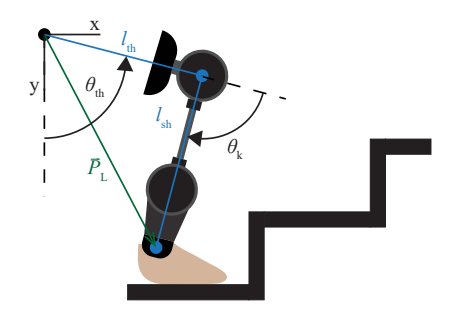


Fig. 1. A two-link planar model of a human leg, with the center of rotation of the hip as the origin. The global thigh angle is denoted as θ_{th} and the relative knee angle is denoted as θ_{k} . l_{th} denotes thigh segment length from the hip center of rotation at the origin to the center of rotation of the knee. Similarly, l_{sh} denotes the shank segment length from the knee center of rotation to that of the ankle. The green vector starting at the center of rotation of the hip and ending at the ankle is denoted as \vec{P}_{L} . This model forms the basis of the thigh feature estimation outlined in (8).

important. In the past, we have assumed that features extracted directly from AB averages of task-specific thigh trajectories will suffice for our control purposes, with either hand-tuning of feature parameters [31], [32], [35] or online updates of these features over multiple steady-state strides [34]. Hand tuning, however, increases acclimation and training time with each new task added to the controller. Online moving-average feature predictions require multiple steady-state strides prior to convergence, which is feasible during treadmill or level ground walking but is prohibitively slow on a short staircase. We, therefore, propose a thigh trajectory feature estimator that generates participant-specific features for each step height that are individualized based on lower limb geometry.

To define a relationship between participant limb geometry and the thigh trajectory features, we model the leg as a floating, planar, serial-link system with two links corresponding to the thigh and shank. We then define $\vec{P}_{\rm L}$ as the vector between the hip and the ankle, shown in Fig. 1. $\vec{P}_{\rm L}$ can be written as

$$\vec{P}_L = \begin{bmatrix} p_L^x \\ p_L^y \end{bmatrix} = \begin{bmatrix} l_{th} \sin(\theta_{th}) + l_{sh} \sin(\theta_{th} - \theta_k) \\ -l_{th} \cos(\theta_{th}) - l_{sh} \cos(\theta_{th} - \theta_k) \end{bmatrix}, \quad (7)$$

where $l_{\rm th}$ and $l_{\rm sh}$ are the thigh and shank lengths, respectively. We simplify our model by making the assumption that the vertical component of our vector, $p_{\rm L}^y$, varies with changes to the thigh and shank length, while the horizontal component, $p_{\rm L}^x$, is constrained to be the same for a given step height, regardless of leg geometry. This is because $p_{\rm L}^x$ at FS is somewhat constrained by the stair geometry. For each step height, γ , we construct an optimization problem to determine the expected thigh trajectory $\theta_{\rm th,\gamma}$, based on the user's thigh and shank length. The optimization minimizes the difference between the average AB $\bar{p}_{\rm L}^x$ and our estimated horizontal component $\hat{p}_{\rm L}^x = l_{\rm th} \sin(\theta_{\rm th,\gamma}) + l_{\rm sh} \sin(\theta_{\rm th,\gamma} - \theta_{\rm k,\gamma}^{\rm AB})$ given normative biological knee angles $\theta_{\rm k,\gamma}^{\rm AB}$.

$$\begin{aligned} & \theta_{\text{th},\gamma}^* = \arg\min_{\theta_{\text{th}}} \|\bar{p}_{\text{L}}^x - \hat{p}_{\text{L}}^x\|_2^2 \\ & \text{subject to } -\frac{\pi}{4} \le \theta_{\text{th}} \le \frac{\pi}{2}. \end{aligned} \tag{8}$$

The constraint ensures the solution is within the expected ROM of the global thigh angle calculated from AB data.

This nonlinear program was implemented in MATLAB and solved using fmincon. The phase variable parameters are then calculated from the expected thigh trajectory.

B. Stance Impedance and Swing Kinematic Controllers

We calculate the joint torque during stance $\tau_{\rm st}$ with an impedance controller where the impedance parameters vary throughout the gait cycle and across step heights. We input the calculated stance phase estimate $\hat{s}_{\rm st}$ from Section III-A1 and a known step height, γ , into an impedance model to determine the joint stiffness K, equilibrium angle $\theta_{\rm eq}$, and damping component B for the impedance torque control law

$$\tau_{\rm st} = m \left(K(s_{\rm st}, \gamma) (\theta_{\rm eq}(s_{\rm st}, \gamma) - \theta) - B(s_{\rm st}, \gamma) \dot{\theta} \right), \quad (9)$$

which is scaled by user mass m. The derivation of the impedance model is presented in Section IV.

During swing, we utilize a proportional derivative (PD) controller to enforce desired, time-invariant joint kinematics known as *virtual constraints* [31]. For each step height γ , a Fourier series is used to model the average AB knee and ankle kinematics θ_k^d and θ_a^d as functions of gait phase s as in [35]. Before calculating the Fourier series we interpolate the desired joint kinematics from [26] as functions of the average phase variable, based on the average thigh kinematics for the associated step height γ in the reference AB dataset. This approach accounts for non-linearities in the average phase trajectory, improving the phase synchronization (and thus the fit) of the estimated joint kinematics to the reference AB trajectory on average [35]. The commanded joint torques at the knee, $\tau_{\rm sw}^k$, and ankle, $\tau_{\rm sw}^a$, are functions of their respective desired joint positions:

$$\tau_{\text{sw}}^{i} = k_{\text{p}}^{i}(\theta_{i}^{\text{d}}(s_{\text{sw}}, \gamma) - \theta_{i}) - k_{\text{d}}^{i}\dot{\theta}_{i}, \tag{10}$$

where $k_{\rm p}^i$ and $k_{\rm d}^i$ are constant proportional and derivative gains for each joint. We utilized viscous damping in order to limit vibrations that naturally arose from a derivative tracking term due to the actuators' minimal inherent viscous losses. Time-based interpolation between $\tau_{\rm st}$ and $\tau_{\rm sw}$ is performed at each FS and TO to ensure a smooth transition as in [36].

IV. STANCE IMPEDANCE MODEL FOR STAIRS

A. Model Definition

Following the framework presented in [36], we build a polynomial-based piecewise-linear impedance model for both the knee and ankle during stair ascent and descent. The model is parameterized by the user's completion fraction of the stance phase $s_{\rm st}$ and the stairstep height γ , where γ is defined over the range $\pm (102 \le \gamma \le 178)$ mm. A negative step height represents stair descent. The model is defined by

$$\begin{bmatrix} K(s_{\rm st}, \gamma) \\ B(s_{\rm st}, \gamma) \\ \theta_{\rm eq}(s_{\rm st}, \gamma) \end{bmatrix} = \begin{bmatrix} c_K(\gamma)^{\top} \\ c_B(\gamma)^{\top} \\ c_{\theta}(\gamma)^{\top} \end{bmatrix} \begin{bmatrix} s_{\rm st}^0 \\ \vdots \\ s_{\rm st}^d \end{bmatrix}, \tag{11}$$

where each task function $c_i(\gamma) \in \mathbb{R}^{d+1\times 1}$ is the product of a matrix of constant coefficients $X_i \in \mathbb{R}^{d+1\times 8}$ and an

interpolation vector $w(\gamma) \in \mathbb{R}^{8\times 1}$, $||w(\gamma)|| = 1$. For example, $c_K(\gamma)$ is defined as

$$c_K(\gamma) = \underbrace{\begin{bmatrix} k_{0,-178} & \dots & k_{0,178} \\ \vdots & \ddots & \vdots \\ k_{d,-178} & \dots & k_{d,178} \end{bmatrix}}_{X_K} w(\gamma), \qquad (12)$$

where, for example, $w(-178) = \begin{bmatrix} 1 & 0 & \dots & 0 \end{bmatrix}^{\top}$ and $w(178) = \begin{bmatrix} 0 & \dots & 0 & 1 \end{bmatrix}^{\top}$. The task functions for damping and equilibrium angle are defined similarly. The model is fully defined when the three parameter matrices X_K, X_B , and X_θ are chosen. Model polynomial orders d=9 and d=4 were chosen for the knee and ankle, respectively, to balance model flexibility with overfitting risk.

B. Model Fitting

To fit our model, we use an optimization-based approach leveraging a dataset of AB steady-state stair ascent and descent [26]. The dataset contains kinematic and kinetic joint information from 24 participants ascending and descending stairs at four step heights $\pm (102 \le \gamma \le 178)$. First, we calculate the inter-participant average kinematics and kinetics for each joint at each step height. For this average, we combine right and left leg joint data assuming symmetry and utilize only the second, full stair stride where a force-plate was available to detect FS and TO. We also calculate the inter-participant average stance phase variable trajectory at each step height.

In principle, our goal in model fitting is to identify the optimal impedance parameter coefficient matrices X_K^*, X_B^* , and X_θ^* that best reproduce the average mass-normalized joint torque trajectories τ in the dataset given the dataset kinematics. Because each column of the parameter matrices only affects the impedance for a single step height, each column can be solved independently and re-assembled for the final model.

1) Optimization Cost Function: Let $x_{k,i}^*$, $x_{B,i}^*$, and $x_{\theta,i}^*$ be the *i*th columns of X_K^* , X_B^* , and X_θ^* , respectively. Similarly, let τ_i , θ_i , and $\dot{\theta}_i$, be vectors of length n of the average dataset torques, joint angles, and joint velocities for the respective step height. Let s_i be a vector containing the average stance phase variable trajectory based on the dataset thigh kinematics and the definitions given in Sec. III-A. This parameterization allows the optimization to account for a potentially nonlinear relationship between our phase variable and normalized time in real-time use. Given these data, we wish to solve the following optimization problem for each step height γ_i based on a modified squared error metric:

$$\{x_{K,i}^{*},x_{B,i}^{*},x_{\theta,i}^{*}\} = \arg\min \parallel \tau_{i} - \hat{\tau} \parallel_{2}^{2} + J \left\|Y_{i}\hat{\tau}_{s}\right\|_{2}^{2}, \quad (13)$$

where

$$\begin{split} \hat{\tau}_s &= K(s_i, \gamma_i) (\theta_{\text{eq}}(s_i, \gamma_i) - \theta_i), \\ \hat{\tau} &= \hat{\tau}_s - B(s_i, \gamma_i) \dot{\theta}_i, \\ J &= 1 \text{ for knee}, J = 0 \text{ for ankle.} \end{split}$$

Here, $Y_i \in \mathbb{R}^{n \times n}$ is a constant diagonal weighting matrix that penalizes the spring torque $\hat{\tau}_s$ in late stance during stair

descent. This matrix $Y_i = \operatorname{diag}(y_i)$ is defined by a piecewise-linear-in-phase weight vector $y_i \in \mathbb{R}^{n \times 1}$. For stair ascent, $y_i = \mathbf{0}^{n \times 1}$. For stair descent, we define y_i for each data point j as

$$y_i[j] = \max\left(0, 1 - \frac{n-j}{n-j_{\text{mid}}}\right),\tag{14}$$

where j_{mid} denotes the data point at the midpoint between when MHE and peak knee torque occur during descent. We added this spring torque penalty to the cost function to encourage the optimization to select solutions where late stance torque is mostly provided through damping. We desire this behavior because, in late stance, the thigh angular velocity is small compared to larger angular velocities at the knee and ankle. Due to our thigh-based phase variable, low thigh velocity results in slowly changing impedance parameters, which may inhibit the desired joint progression rates if dominated by spring-like behavior. This cost function modification is also inspired by the damping behavior exhibited by passive prosthetic knees, which have been shown to emulate AB knee kinematics and kinetics during stair descent [17], [18].

However, the optimization problem (13) is non-convex, meaning that globally optimal solutions cannot be guaranteed or solved for efficiently. Our past work [36] showed that by making the substitution

$$K(s_{\rm st}, \gamma)\theta_{\rm eq}(s_{\rm st}, \gamma) = \delta(s_{\rm st}, \gamma) = w(\gamma)^{\top} X_{\delta}^{\top} \begin{bmatrix} s_{\rm st}^{0} \\ \vdots \\ s_{\rm st}^{2d} \end{bmatrix}$$
(15)

and treating the $X_\delta \in \mathbb{R}^{2d+1 \times 8}$ coefficients as new, independent parameters similar to [42], the problem can be reduced to a convex quadratic program [36]. Specifically, if we define a decision vector $x \in \mathbb{R}^{4d+3 \times 1} = \left[x_{K,i}^\top, x_{B,i}^\top, x_{\delta,i}^\top\right]^\top$, where $x_{\delta,i}$ are the columns of X_δ , the cost function defined in (13) becomes linear in the unknown parameters. Let the jth column in $\alpha \in \mathbb{R}^{4d+3 \times n}$ be defined as

$$\alpha[j] = -[\theta_{ij}s_{ij}^{0}, \dots, \theta_{ij}s_{ij}^{d}, \dot{\theta}_{ij}s_{ij}^{0}, \dots, \\ \dot{\theta}_{ij}s_{ij}^{d}, -s_{ij}^{0}, \dots, -s_{ii}^{2d}]^{\top},$$
(16)

where subscript j denotes the jth component in each vector of length n. Let the jth column in $\beta \in \mathbb{R}^{4d+3\times n}$ be defined as

$$\beta[j] = \left[-\theta_{ij} s_{ij}^0, \dots, -\theta_{ij} s_{ij}^d, \mathbf{0}^{1 \times d}, s_{ij}^0, \dots, s_{ij}^{2d} \right]^\top. \tag{17}$$

Then, the cost function L(x) can be written as the quadratic function

$$L(x) = \tau_i^{\top} \tau_i - f^{\top} x + x^{\top} H x, \tag{18}$$

where

$$H = \alpha \alpha^{\top} + \beta Y_i Y_i \beta^{\top}, \quad f = 2\alpha \tau_i. \tag{19}$$

2) Optimization Constraints: To prevent overfitting we added a diagonal regularization matrix $\Lambda \in \mathbb{R}^{4d+3\times 4d+3}$ to penalize the L_2 norm of x. The diagonal entries in Λ corresponding to the regularization weights on $x_{k,i}$ and $x_{b,i}$ were $1e^{-4}$ for ascent and $1e^{-5}$ for descent. For weights on $x_{\delta,i}$, the diagonal entries were $1e^{-10}$ for ascent and $1e^{-7}$ for descent. These hyperparameters were chosen during model fitting to produce a smooth model to capture general behavior

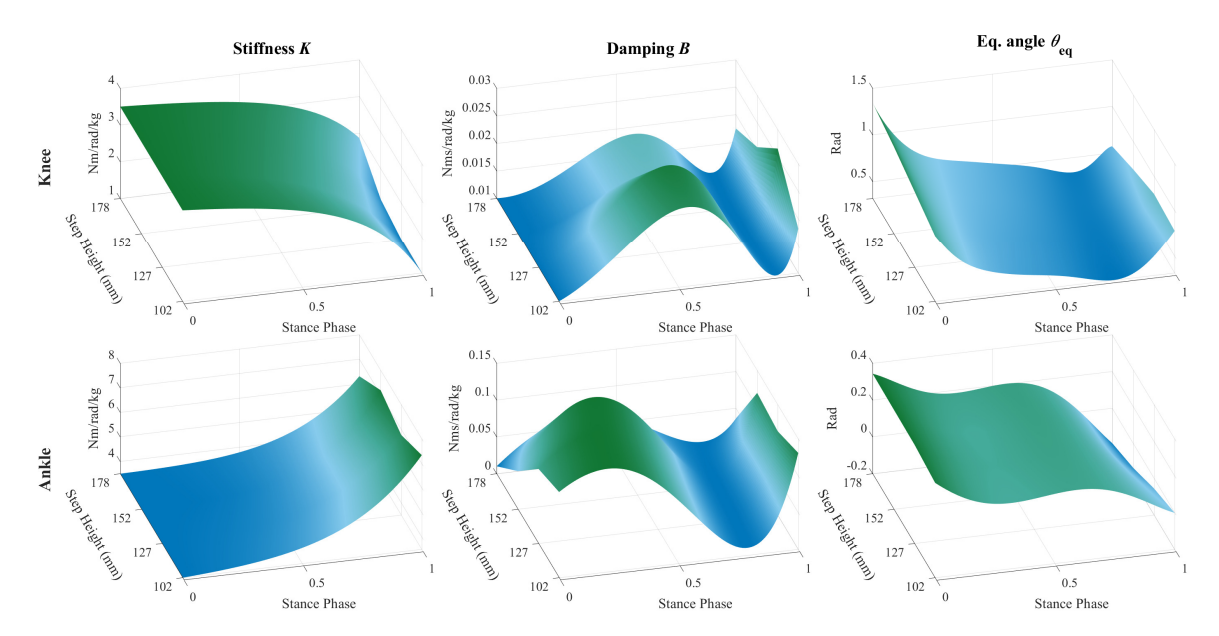


Fig. 2. Plots of the calculated stair ascent impedance functions for stiffness $K(s_{\rm st},\gamma)$, damping $B(s_{\rm st},\gamma)$, and equilibrium angle $\theta_{\rm eq}(s_{\rm st},\gamma)$ for the knee and ankle over the range of step height configurations from $\pm (102 \text{ to } 178) \text{ mm}$.

without overfitting to the training data. Regularization also limited undesirable solutions such as an excessively large spring torque balanced by an excessively large damping torque in the opposite direction.

We added constraints on x such that $Ax \leq b$ where $A \in \mathbb{R}^{n \times 4d + 3}$ and $b \in \mathbb{R}^{n \times 1}$ to ensure that stiffness $K(s_{\rm st}, \gamma)$ and damping $B(s_{\rm st}, \gamma)$ remained within ranges that were both physiologically realistic and feasible for the prosthesis to perform. The details of the construction of A are omitted for brevity, but are available in [36]. Due to differences in the desired joint behavior for the ankle and knee over both ascent and descent, a different set of constraints was used for each activity and joint combination (Table SI). A minimum FS stiffness was chosen for each joint based on pilot trial feedback, as participants were accustomed to the stiff behavior of their take-home device at the start of the gait cycle. Across both ascent and descent, torque from damping was constrained to a maximum of 0.14 Nms/rad/kg due to limitations of velocity filtering methods utilized in the powered prosthesis.

3) Quadratic Program: Minimizing the cost function L(x) along with the regularization penalty $x^{\top} \Lambda x$ subject to the inequality constraints yields the final quadratic program (QP):

minimize
$$x^{\top}(H+\Lambda)x - f^{\top}x$$
,
subject to $Ax \le b$. (20)

The positive offset $\tau_i^\top \tau_i$ originally in (18) is neglected without loss of generality. We solved this QP for each step height and joint using the MATLAB Optimization Toolbox (R2022b). To recover the original model's equilibrium angle function $\theta_{\rm eq}(s_{\rm st},\gamma)$ in (11), we performed a least-squares fit of $\delta(\chi_p,s_{\rm st})/K(\chi_p,s_{\rm st})$ to a d-th order polynomial at each incline. The polynomial order was sufficiently high enough to prevent significant approximation error. The impedance models from the training step heights $\gamma=\pm\{102,127,152,178\}$ mm are shown in Fig. 2 for ascent and Fig. S2 for descent.

C. Model Evaluation

To quantify the impedance parameter model's reconstruction error, we calculated $\hat{\tau}$ for the knee and ankle over the interparticipant average kinematic data for each training step height in the AB dataset using the fit impedance model. We then calculated the root mean squared error (RMSE) in joint torque for each step height. Note that the RMSE is distinct from the cost function minima. Across all tasks, the average RMSEs were $e_{\rm k}=0.11\pm0.1$ Nm/kg and $e_{\rm a}=0.06\pm0.03$ Nm/kg.

V. AMPUTEE EXPERIMENTS

A. Methods

The biomimicry of the HKIC framework for stair ascent and descent was experimentally assessed with two amputee participants (see Table SII for participant details). The aforementioned continuously varying impedance model, generated a-priori, was utilized across all experiments. The experimental protocol was approved by the University of Michigan Review Board (HUM00166976). The proposed control method was implemented on a backdrivable, powered knee-ankle prosthesis shown in Fig. 3 and designed in [13]. This prosthesis features a quasi-direct drive, low inertia actuation design that allows for open-loop joint impedance control and high-bandwidth position control. A licensed prosthetist fit the robotic prosthesis to the participants, ensured proper alignment, and supervised the experiment for participant safety. Participants also wore a ceiling-mounted safety harness.

The participants each completed the experimental protocol once with the robotic prosthesis. For comparison, participant two (P2) also completed the same experimental protocol on a separate testing day with his passive device (Ottobock Genium X3) due to his unique ability to perform step-over-step stair ascent. Photos of the experiment are shown in Fig. 3 and videos are available in the supplementary materials.





(a) P1: Stair Ascent

(b) P2: Stair Descent

Fig. 3. Photos of above-knee amputee (AKA) participants P1 and P2 performing stair ascent and descent. (a) shows P1 in the stair ascent FS configuration and (b) shows P2 in the stair descent FS configuration.

The experimental protocol investigated the performance of the HKIC controller and passive device during stair ascent and descent at four step heights on an adjustable staircase. Step heights of 102 mm (4 in.), 127 mm (5 in.), 152 mm (6 in.), and 178 mm (7 in.) were chosen to comply with the Americans with Disabilities Act (ADA) [40]. Ten trials were performed at each step height, where each trial comprised one ascent and one descent of the staircase. A one-minute break was given between trials, and a 5-minute break was given after the fifth trial to mitigate any effects of fatigue. Joint kinematics and kinetics were recorded from the robotic prosthesis. An infrared motion capture system (Vicon Ltd. Oxford, UK) collected sound limb and passive device kinematics.

Before the HKIC experiment day, each participant attended an acclimation session during which they were given an overview of the high-level functionality of the controller and given time to acclimate to stair ascent and descent at a moderate step height of 152 mm (the nominal ADA-compliant step height [18]). On the day of the experiment, we gave the participant time to acclimate to the controller at each step height before performing a set of trials. Participants were encouraged to limit body weight support on the handrails to maximize the load on the device and to ascend and descend the stairs at a consistent, comfortable pace. Note that no hand-tuning of controller parameters was done for either participant.

P1 completed all step height configurations with the powered leg, whereas P2 was unable to do the 178 mm configuration. The participant noted discomfort at the largest step height due to the mass of the powered leg and had trouble lifting it into the starting configuration for stair ascent (see Fig. 3 for the example configuration). We suspect that the discomfort was exacerbated by the participant's shorter residual thigh, with the large distal mass of the device creating a significant bending moment on the socket-limb interface. Due to this issue, we present only data from the lower three step height configurations for P2 using the powered leg.

A similar experimental protocol was followed on a different day for P2's passive device trials. Since the participant was familiar with the prosthesis' stair ambulation behavior from daily use, there was no session dedicated to acclimation prior to the experiment. The participant used a specific hip motion to activate and maintain stair ascent behavior with their take-home device. However, the device occasionally failed to trigger stair ascent mode causing the participant to kick the stair before having to re-attempt the motion. These trials

were discarded and additional trials were performed until ten successful trials were performed at each step height.

Kinematic and kinetic data were compared between the robotic prosthesis running our novel controller (HKIC), the passive device (PAS), and the able-bodied (AB) reference. The AB reference represents the inter-subject average steady-state stride at each step height configuration from the open-source biomechanics dataset [26] used to train our impedance model. We designated the second full stair stride as the steady-state stride for both the HKIC and PAS trials. Biomechanics results that are noteworthy (e.g., within a standard deviation of the AB reference) are **bolded**. Additional results and figures are available in the supplementary materials.

B. Stair Ascent Results

- 1) Phase Variable: Fig. 4 shows the resulting phase variable for each participant, showing its ability to parameterize the gait cycle and the effectiveness of the geometry individualization. Both participants' phase variables (Fig. 4a) showed monotonic behavior with little to no saturation for the majority of the gait cycle. However, phase saturation occurred for P1 towards the end of the gait cycle (see Discussion). The measured thigh angle features for both participants at foot-strike and MHF (Fig. 4b,4e) closely matched the predicted feature angles from the geometry individualization. The thigh angles at MHE and TO (Fig. 4c,4d) were smaller than the predicted values and showed larger variability for both participants.
- 2) Kinematics: Fig. 5 shows the intra-participant kinematic trajectories over stance and swing for the HKIC and PAS kinematics compared to the AB reference. The kinematic trajectories at both the knee and ankle joint produced by the HKIC at steady-state resembled that of the inter-participant AB kinematics at each step height tested. The PAS kinematics at the knee resembled the AB reference in both shape and trend but reached levels of extension and flexion that are not seen in biological data. While this extreme knee ROM likely contributed to the larger amount of toe-clearance exhibited by the PAS device to prevent toe-stubs (see supplementary video), a non-biomimetic thigh motion was required to achieve this. Throughout the gait cycle, the PAS ankle had a limited range of motion and was unable to provide biomimetic plantarflexion and dorsiflexion.

Table SIII shows the kinematic ROM of the HKIC, PAS, and AB joints across step heights. At the nominal step height of 152 mm, the HKIC achieved average peak knee flexion angles of **94.13** deg for P1 and **93.58** deg for P2, allowing step clearance during swing without toe stubbing. Unlike the PAS knee, which reached an excessive peak flexion angle of 122.39 deg, both participants' peak knee flexion with the HKIC were within one standard deviation of the AB peak of 96.31±5.4 deg. At FS, the HKIC produced average knee angles of **69.42/69.21** deg for P1/P2 compared to the PAS knee angle of 59.93 deg and AB knee angle of 68.86±4.33 deg. At the ankle joint, the HKIC achieved dorsiflexion angles of **24.04/26.87** deg during stance. The PAS, in contrast, showed a reduced ankle dorsiflexion angle of 11.57 deg compared to the AB dorsiflexion angle of 25.42±4.01 deg. Ankle plantarflexion at

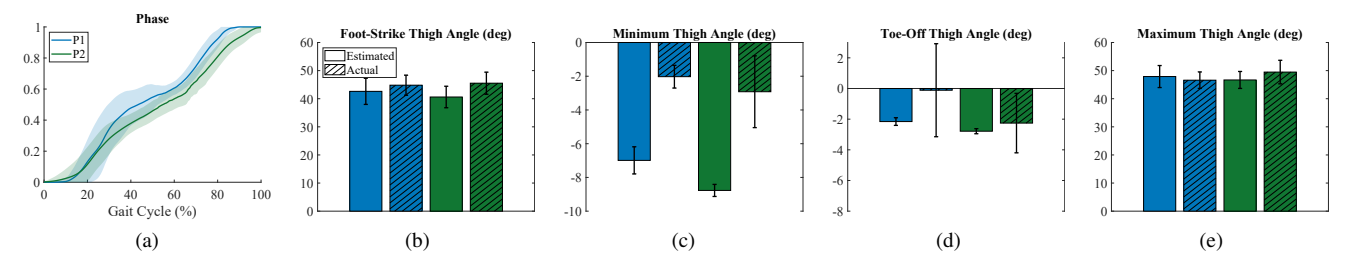


Fig. 4. Stair ascent plots of (a) phase variable trajectory averaged over step heights for both participants (shaded regions represent \pm 1 standard deviation), as well as comparisons between each participant's estimated and experimental thigh features averaged over all four stair configurations at foot-strike (b), MHE (c), TO (d), and MHF (e). Error bars denote \pm 1 standard deviation on either side of the mean. P1 is denoted in blue and P2 is denoted in green. In plots (b-e), bars with hatch lines denote experimental results while bars without hatching denote the estimated thigh features utilized in the control of the device. The phase variables for both participants showcased monotonic behavior with little to no saturation at the end of the gait cycle.

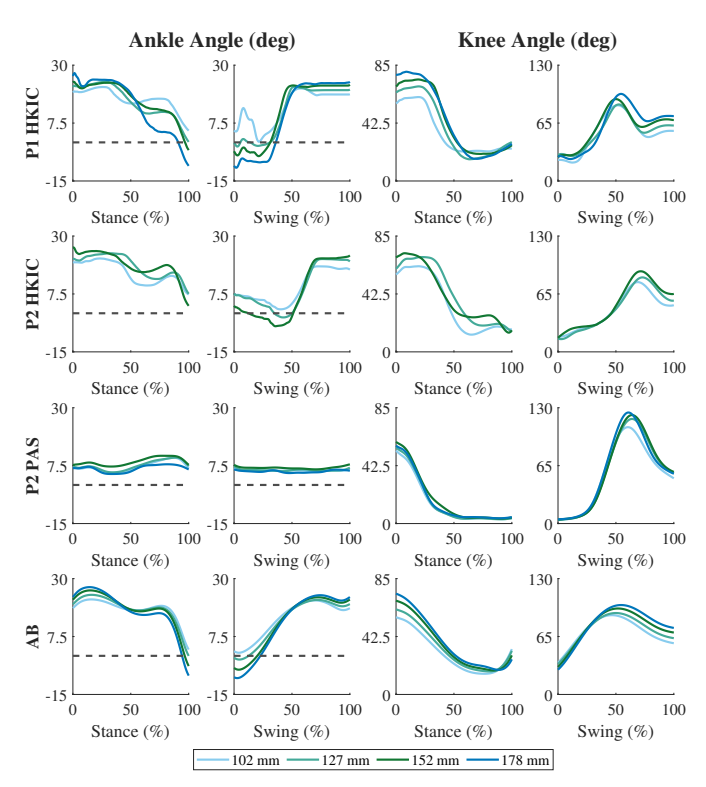


Fig. 5. Plots of stair ascent intra-participant average joint kinematics over stance and swing for HKIC and PAS vs. AB kinematics across step height configurations. The dashed line in these plots denotes 0 degrees on the y-axis. The HKIC controller produced kinematics that replicated the shape and behavior of the AB joint trajectories. While P2's passive device kinematics at the knee resemble AB knee kinematics, the ankle is unable to replicate AB plantarflexion and dorsiflexion. Note that P1 was unable to perform PAS step-over stair ascent, so their PAS kinematics are not plotted.

the end of stance, which is important for achieving push-off, was **-7.6/-5.83** deg for the HKIC compared to the AB reference of -4.35 ± 7.12 deg. The PAS ankle was unable to plantarflex, remaining in a dorsiflexed configuration with a minimum ankle angle of 5.78 deg.

3) Kinetics: Fig. 6 reports the intra-participant average and individual trial joint kinetic trajectories for the 102 mm and 152 mm step heights, representing shallow and steep staircase configurations. We focus on the stance period where the impedance controller torques determine the environmental interaction experienced by the user. The individual trials were included to showcase how the HKIC was able to accommodate changes in stride timing while providing joint torques that are

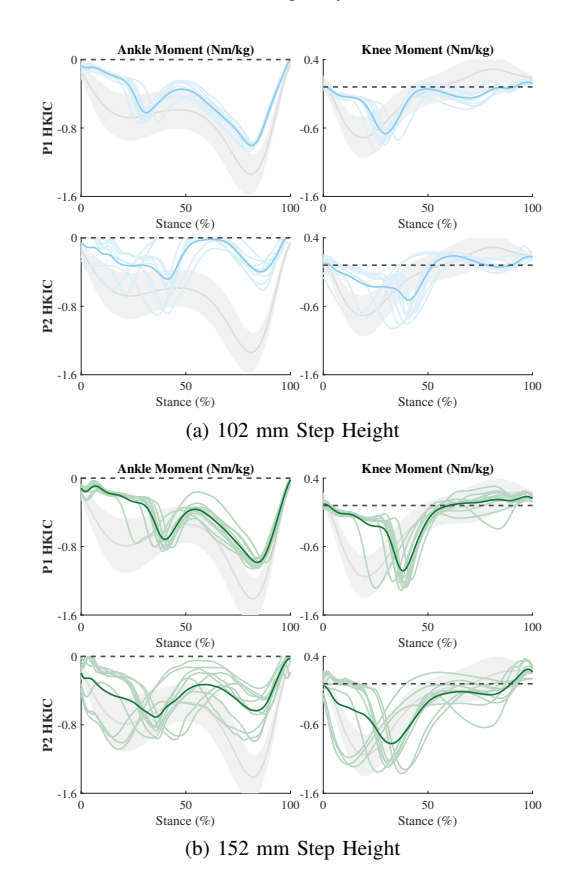


Fig. 6. The participants' individual trial and intra-participant average joint torques for stair ascent at the 102 (a) and 105 (b) mm step height configurations in comparison to the mean (± 1 standard deviation) AB reference torque profiles, denoted in grey. The average torque for each joint is denoted with an opaque color while the individual trial or standard deviation curves are denoted with a lighter color. The dashed black line denotes 0 Nm/kg on the y-axis. The HKIC produced smooth kinetic trajectories at both step heights, increasing knee extension torque and ankle push-off torque as step height increased.

similar in shape and magnitude to the AB reference. Pertinent features of the joint kinetics across all step heights are shown in Table SV.

At the step height of 102 mm (see Fig. 6a), the mean HKIC knee kinetic trajectories of both participants resembled that of the AB references, achieving peak moments of **-0.84/-0.81** Nm/kg for P1/P2. At the ankle, both participants match the AB reference in torque magnitude in early to mid-stance but applied less torque during push-off (**-1.03/-0.72** Nm/kg

for P1/P2). At the step height of 152 mm (see Fig. 6b), the mean HKIC knee torque trajectories of both participants are similar to that of the AB reference trajectory. The participants' average peak knee torques were within a standard deviation of the AB average with peaks of -1.22/-1.21 Nm/kg. Similar to the 102 mm step height, both participants' ankle torque matched that of the AB reference throughout the majority of stance but fell short at pushoff. However, the pushoff torque at the ankle on the 152 mm configuration increased relative to the 102 mm configuration to help facilitate the larger stair rise with -0.96 Nm/kg for P2, while remaining consistent for P1 at approximately -1.02 Nm/kg. At both step height configurations, P2's HKIC torque trajectories showed varying stance progression and peak torque timings, whereas P1's results showed more consistent stance progression and peak torque timing across trials.

The HKIC provided the net-positive work necessary for stair ascent (see Table SV in the supplementary material), producing biological trends similar to able-bodied data as step-height varied. The knee joint imitated biological work particularly well, producing an average of 0.61/0.58 J/kg at the knee for both participants at the 152 mm configuration, which is within one standard deviation of the AB reference value of 0.51±0.18 J/kg. Similarly, at 102 mm, the knee provided 0.33/0.32 J/kg, again within a standard deviation of the AB reference of 0.34 ± 0.14 . The ankle joint produced, on average, lower net-positive work than the AB reference for both participants, but P1's ankle work was within a standard deviation of the AB reference for all step heights. Despite the lower average net-positive work, the ankle joint produced biological trends similar to the knee, increasing from **0.15**/0.06 J/kg at 102 mm to **0.24**/0.14 J/kg at 152 mm.

C. Stair Descent Results

- 1) Phase Variable: Fig. 7 highlights phase and thigh feature prediction results over all stair descent trials. P1's average phase variable exhibited monotonic behavior for the majority of the gait cycle but was saturated at the start and during the last tenth of the gait cycle. This saturation at the end of the stride is likely caused by the larger MHF angle reached by P1 in comparison to the predicted phase variable parameter, as shown in Fig. 7e. P2 similarly showed phase saturation for the first ten percent of the gait cycle but then exhibited monotonic behavior for the majority of the stride. At foot-strike (Fig. 7b) the predicted thigh angle parameter was within a standard deviation of P2's foot-strike angle. P1's average MHE angle similarly stayed within a standard deviation of predicted thigh angle. At TO, there was a large discrepancy between P2's predicted thigh angle and the experimental results, implying early TO from the participant. While P1's average TO thigh angle was within a standard deviation of the predicted value, the large standard deviation points to inconsistency in TO angle across trials and activities.
- 2) Kinematics: Fig. 8 showcases the intra-participant kinematic trajectories over stance and swing for the HKIC and PAS kinematics compared to the AB reference. Across the four step heights considered in this study, the stance kinematic

trajectories produced by the HKIC at both the knee and ankle joints at steady-state resembled that of the inter-participant AB kinematics. While P2's swing kinematics resembled the AB reference, P1's swing kinematics followed AB trends but progress rapidly at the beginning of swing and then remained almost constant for the latter half of swing. This behavior was likely a result of the phase saturation at this point in the gait cycle, shown in Fig. 7a. Both participants exhibited knee kinematics with similar profiles to the AB reference for the majority of stance. However, the PAS ankle had a limited range of motion and was unable to provide biomimetic plantarflexion and dorsiflexion. To compensate for the minimal ankle ROM, the participant placed their foot at the end of the step, using the edge as a pivot point to achieve knee flexion.

Table SIV showcases the kinematic ROM of the HKIC, passive, and AB joints over step heights. At the nominal 152 mm step height, the HKIC achieved biomimetic levels of knee flexion during swing to avoid toe-stubbing with average peak knee flexion angles of 91.38 ± 3.00 deg for P1 and 88.40 ± 2.39 deg for P2. At FS, the HKIC reached knee extension angles of 20.38/17.06 deg for P1/P2, within one standard deviation of the AB reference of 19.96±6.40 deg. The HKIC ankle reached dorsiflexion angles of 30.75/36.63 deg during stance and plantarflexion angles of -10.08/-7.48 deg at FS. Despite showing biological trends over step height for stair descent, the PAS knee showed higher kinematic errors at key points in the gait cycle compared to the HKIC (Table SIV). The PAS ankle similarly underperformed in comparison to both the HKIC and AB reference due to its limited ROM, forcing P2 to perform compensatory lunging and edge-of-step pivot behaviors that likely negatively impacted PAS knee performance.

3) Kinetics: In stair descent, both participants' HKIC ankle and knee joint kinetic profiles resembled that of the AB reference. Fig. 9 reports the intra-participant average and individual trial kinetic trajectories at both joints for the 102 mm and 152 mm step heights. Kinetic performance across all step height configurations is shown in Table SVI.

At the minimum step height of 102 mm, the HKIC reached biomimetic peak knee extension torques of -0.83±0.06 Nm/kg for P1 and -0.77±0.05 Nm/kg for P2. The HKIC also reached biomimetic peak torques at the ankle for both participants (-0.76/-0.81 Nm/kg). At the nominal step height, the peak torque was -1.05/-0.94 Nm/kg at the knee and -0.84/-1.06 Nm/kg at the ankle for P1/P2. Across these step height configurations, both participants' peak joint torques were within a standard deviation of the AB references and generally increased in magnitude with step height following biological trends.

During descent, the HKIC provided controlled negative work at the joints. The HKIC knee joint performed -0.56/-0.33 J/kg at the nominal 152 mm step height and -0.34/-0.15 J/kg at the 102 mm step height, which were less than AB. The HKIC results for both participants followed biological trends of increasing magnitude of work with increased step height. On the other hand, the HKIC ankle provided biomimetic negative work of **-0.3/-0.39** J/kg at 152 mm and **-0.22/-0.27** J/kg at 102 mm, which are within a standard deviation of the reference AB values -0.44±0.15 J/kg and -0.26±0.13 J/kg.

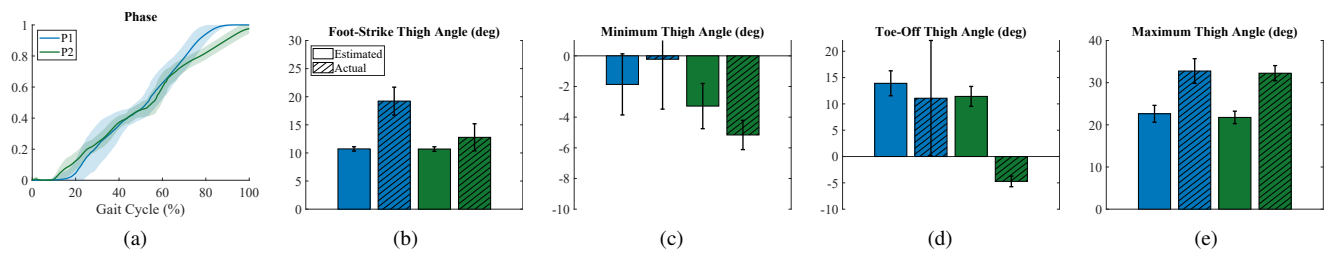


Fig. 7. Stair descent plots of (a) inter-step height mean phase variable for both participants (shaded regions represent \pm 1 standard deviation), as well as comparisons between each participant's average (\pm 1 standard deviation) estimated and experimental thigh features over all four configurations at foot-strike (b), MHE (c), TO (d), and MHF (e), during stair descent. P1 is denoted in indigo and P2 is denoted in green. In plots (b-e), bars with hatch lines denote experimental results while bars without hatching denote the estimated thigh features utilized in the control of the device. The phase variables for both participants showcased monotonic behavior during the majority of the gait cycle with saturation at the start of the gait cycle.

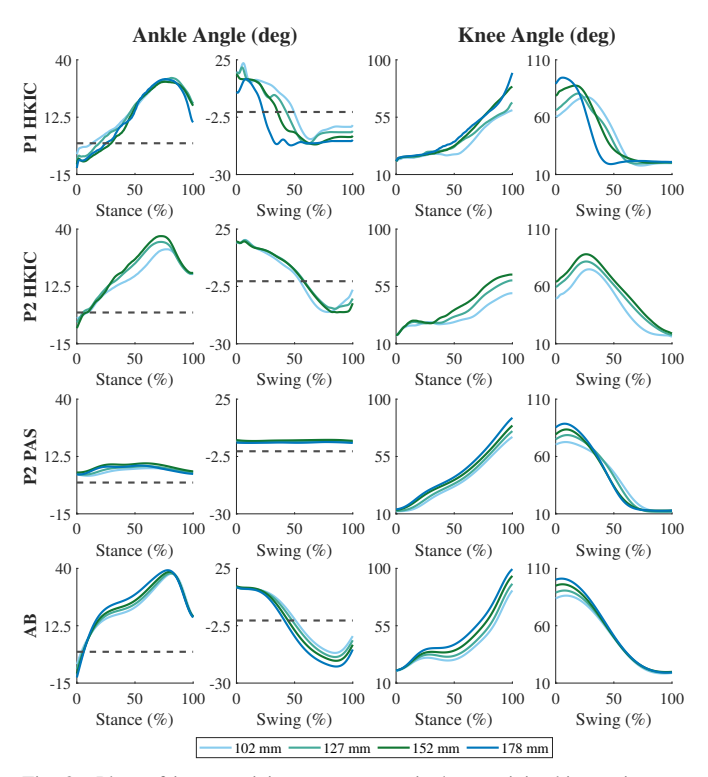


Fig. 8. Plots of intra-participant average stair descent joint kinematics over stance and swing for powered and passive devices vs. AB kinematics across step height configurations. The dashed line in these plots denotes 0 degrees on the y-axis. The HKIC controller produced kinematics that replicated the shape and behavior of the AB joint trajectories. While P2's passive device stance kinematics at the knee resembles AB knee kinematics, the ankle is unable to replicate AB plantarflexion and dorsiflexion.

VI. DISCUSSION

A. HKIC Performance

The indirect-volitional HKIC was able to handle variations in stance progression and timing differences between different trials, step height configurations, and participants. The average phase progression during stair locomotion was monotonic throughout the majority of the gait cycle for ascent and descent (Figs. 4 & 7). This monotonic behavior, along with the similarity of many observed and estimated thigh features, points to the strength of the thigh feature estimation paradigm proposed in this work.

However, P1 exhibited phase saturation over the last ten percent of the stair descent stride. Normally, saturation or

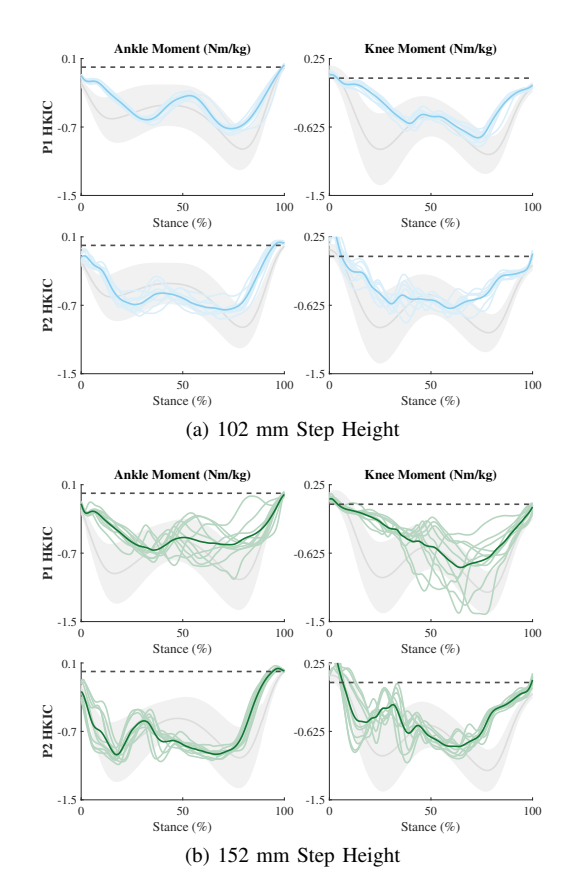


Fig. 9. The participants' individual trial and intra-participant average joint torques for stair descent at the 102 (a) and 152 mm (b) step height configurations in comparison to the mean (±1 standard deviation) AB reference torque profiles, denoted in grey. The average torque for each joint is denoted with an opaque color while the individual trial or standard deviation curves are denoted with a lighter color. The dashed black line denotes 0 Nm/kg on the y-axis. The HKIC controller produced kinetic trajectories that resembled AB data at both step heights, increasing knee extension torque in mid-to-late stance and ankle torque for early-stance energy absorption as step height increased.

pauses in phase can cause desynchronization and can lead to trips, falls, or oscillations. However, to promote user confidence at FS, we biased the phase variable definition to saturate early so the prosthetic joints would arrive at their FS configuration early as in [36]. During stair descent trials, P1 often waited at MHF for the feed-forward behavior of the phase variable to bring the knee to an extended position before proceeding with FS. P2 exhibited a similar waiting behavior

at MHF but was more consistent in synchronizing the feedforward phase completion with FS, resulting in little to no phase saturation. This could explain why an increased FS thigh angle was observed for P1 but not for P2 (Fig. 7b). The small pause in P1's phase variable is the likely cause of their abnormal swing kinematic progression during stair descent (Fig. 8). While these kinematics may not exactly match the progression of the AB reference when plotted over normalized swing time due to saturation or non-linearities in phase, this behavior showcases the indirect-volitional benefits of our control approach by allowing user stride progression to dictate leg behavior, synchronizing the user and device.

There were significant discrepancies and/or variations in measured vs. predicted thigh features at TO (Figs. 4d & 7d). This may point to premature TO by the participants due to compensatory habits that they have developed from their passive devices. This early TO relative to the predicted angles resulted in limited torque provided at the ankle at push-off and subsequently below-nominal ankle work during stair ascent, as well as less knee flexion exhibited by P2 during stair descent. Another possible explanation for this discrepancy is that the average AB data used to estimate thigh features does not fully represent the individual behavior of the participants (see Section VI-C).

For both ascent and descent, the HKIC followed biological trends seen in AB stair locomotion, producing knee extension and ankle plantarflexion torques during stance that increased with step height. In swing, both participants also achieved biomimetic levels of knee flexion with the HKIC that allowed for clearance of the following step without toe-stubbing or tripping. During stair ascent, the HKIC produced the necessary joint torques (Fig. 6) at the knee and net-positive work at both joints for multiple step height configurations (Table SV), following biological trends of increasing joint work and peak torque with increasing step height. The HKIC also produced kinematics (Fig. 5) that resembled the AB reference data. The HKIC provided biomimetic plantarflexion angles in tandem with push-off torques at the ankle, which was unachievable with the PAS due to its limited ROM (Table SIII).

In stair descent, the HKIC enabled biologically-similar kinematics (Fig. 8) and kinetics (Fig. 9) at the ankle, producing peak plantarflexion torques within a standard deviation of the AB reference across step heights. At the nominal 152 mm step height, the HKIC provided biomimetic, controlled negative work at the ankle (Table SVI) and allowed biomimetic levels of ankle plantarflexion at FS, exhibiting toe-strike behavior and energy dissipation [1]. Across step height configurations, the HKIC showed biological trends of increasing magnitude of ankle work with step height. The PAS was unable to provide the same level of ankle plantarflexion, resulting in a heel-strike behavior at the beginning of stance that does not allow for the same absorption of energy [9], [18]. Instead, passive device users must compensate with their residual hip or contralateral limb [17]. The HKIC also reached biological peak knee torques for both participants, which allowed for controlled negative work and support that characterize AB stair descent during mid to late stance. However, the torque provided at the knee in early stance was constrained due to continuity requirements in the optimization and hardware limitations (see Section VI-C). Despite this limitation, the peak knee torque and work provided by the HKIC generally followed biological trends of increasing torque and work magnitudes with increasing step heights.

During our experimental sessions, we received positive qualitative feedback from both participants. P1 voiced a preference for the ability of the HKIC to perform step-over stair ascent, an activity they are unable to perform with their PAS device. P2 voiced a preference for stair descent due to the support provided by the HKIC; note that P2 was already capable of a modified step-over ascent using their passive device. Both participants found it helpful that the HKIC did not require them to perform the compensatory lunging behavior they needed to use during passive device stair descent. We noted that P1 acclimated quickly to stair ascent but struggled more with stair descent due to 1) the tendency to perform their accustomed compensatory lunging behavior and 2) a hesitancy to trust the device to support them as they neared terminal stance. P2, on the other hand, acclimated quickly to stair descent but took more strides to acclimate to stair ascent. In particular, it took time for P2 to learn to avoid the compensatory hip whipping motion that they use to perform step-over stair ascent with their passive device.

B. Comparison to the State of the Art

The closest approach for indirect volitional knee-ankle prosthesis control over stairs is the method proposed by the Utah Bionic Engineering Lab (BEL) in [39], though for stair ascent only. Rather than using data-driven optimization, the BEL control approach uses hand-tuned heuristics to modulate stance kinetics and swing kinematics. Notable advantages of the BEL controller include the ability to 1) handle multiple gait patterns such as step-to, step-over, and two-step stair ascent, and 2) automatically adapt to user behavior over different step heights (specifically 102 mm and 178 mm) within the ADA-compliant range. On the other hand, our data-driven HKIC control approach was only designed for the traditional step-over gait pattern and cannot adapt to changes in step height or user gait without the use of a high-level classifier.

However, our HKIC approach has several advantages over the BEL approach. In particular, our controller exhibited biologically similar results across stairstep heights, whereas the BEL approach was not compared to biological reference data or evaluated for biomimicry. Another limitation of the BEL approach is that it was only validated with one experienced participant. Both controllers show biological trends in stair ascent at the knee, with maximum flexion, peak torque, and work scaling with step height. However, the BEL approach was only validated at two of the four step heights validated in this work. Unlike the BEL approach, the HKIC approach does not rely on hand tuning of participant-specific controller parameters. The most notable difference between the BEL and HKIC control approaches is the HKIC extends to both stair ascent and descent, whereas the BEL heuristic approach is limited to just performing stair ascent.

C. Limitations and Future Work

Our study was limited to only two amputees participating in a single experiment session with a short acclimation period. Future work could incorporate more acclimation time, as our participants noted that they often felt more comfortable on the powered device at the end of the experimental session compared to the start. Further improvements can also be made to our acclimation training approach following the outlined training guidelines seen in [43].

The impedance model may have also limited kinetic performance at the knee joint during stair descent. Due to the continuous nature of our model parameters, torque from stiffness must be sacrificed at the start of the gait cycle to achieve the necessary late-stance damping at the knee. A higher-order model could be used to reduce this limitation, but at the risk of introducing too many degrees of freedom in the optimization and overfitting. This limitation may explain why both participants achieved biomimetic peak knee torques during mid to late stance yet performed less total work (Figs. 9 & Table SVI). It is also possible that using different basis functions for the knee could mitigate this issue. Further, the powered leg used in this study was limited in its ability to provide biomimetic damping torques at both joints during stair descent due to the implemented velocity filtering methods.

The supplemental video shows that P2 often completed trials faster with his take-home device than with the powered one. We hypothesize that one factor in this speed discrepancy is the powered prosthetic leg used in the experiment, which is much heavier and relatively unfamiliar compared to the users' passive devices. However, it is possible that the HKIC provides other clinical benefits whose value outweighs this decrease in speed, such as increased endurance [44]. We hope to understand these clinical trade-offs better in future work and to investigate the HKIC approach with lighter-weight powered prostheses capable of accurate impedance control that may be less detrimental to user agility.

Thigh feature estimation based on participant geometry showed promise across both stair ascent and descent, though discrepancies at TO and MHF during stair descent demonstrate a need for improvement and further evaluation. This offline estimation method may also limit the controller's performance because it does not adapt online to the participant's behavior. These limitations could potentially be addressed by automated tuning of parameters for individual users, such as the methods investigated in [45], and online feature adaptation over multiple strides as in [36].

The presented modeling and feature estimation methods assume the inter-subject averages of the AB dataset adequately represent the behavior of our participants. However, individuals' kinetics and kinematics are known to vary from the mean [46]. Variation can also be seen by comparing the different datasets utilized across the field of powered-prosthetic control, whether due to participant individuality or the margin for error in data capture. For example, the raw dataset used in this work [26] exhibits a positive offset in ankle ascent kinematics and knee descent kinematics in comparison to other biomechanical studies [25], [27]. As a result, our impedance parameter model

and thigh feature estimation paradigm may be biased toward increased positive joint flexion. This could explain the early TO exhibited by P2 during stair descent (Fig 7d).

Though our presented results are promising, there are multiple avenues for improving our control approach's performance and overcoming the aforementioned limitations. Previous work has shown that joint kinematics can vary greatly between individuals when performing the same activity [27], [45], [46]. Our impedance model is built to replicate average joint kinetics given average joint kinematics, but the variance in observed stair-climbing patterns suggests that individualized models may be more appropriate. Initial clinically-viable individualization methods have been proposed for data-driven models similar to our HKIC model [47], which may improve the controller's performance. Possible modifications include increased push-off torque to help overcome the weight of the device or increased knee flexion to avoid potential toestubbing without the need for compensatory thigh motions. Future work must also be done to implement some form of real-time step height estimation to improve phase parameter and model estimations.

Finally, there is compelling work to be done on the unification of our HKIC controller and phase variable definitions across activities of daily living. Future studies should focus on modeling impedance and kinematics for transitions between HKIC models (*i.e.*, walk to stair ascent), as well as investigating the clinical benefits of a unified HKIC-controlled paradigm compared to the performance of passive devices.

VII. CONCLUSION

This work presented a data-driven stair ascent and descent controller designed to work across a variety of step heights. This controller involved improvements to the phase estimation method over previous work [35], [36], including thigh angle feature estimation based on the user's limb segment lengths. Two AKA participants demonstrated the controller's ability to provide biologically similar joint kinematics and kinetics across multiple step heights without impedance or phase variable parameter tuning. The HKIC showed improvements over a participant's passive device, particularly at the ankle due to the powered ankle's ability to provide the necessary plantarflexion. The experiments also showcased the controller's capacity to provide appropriate amounts of both positive/negative work during stair ascent/descent as step height varied. This control method can be integrated with other phase-based control methods in future work to enable more biomimetic amputee locomotion over the varying activities of daily life.

ACKNOWLEDGEMENTS

The authors thank Emily Keller, Shihao Cheng, Curt Laubscher, Emma Reznick, Hannah Frame, and Albert Lee for help with experiments, data processing, or paper editing. We also thank our participants for their time and Leslie Wontorcik, CP, and Nicholas Wanczyk for providing clinical support.

REFERENCES

- B. Mcfadyen and D. Winter, "An integrated biomechanical analysis of normal stair ascent and descent," *J. Biomech.*, vol. 21, pp. 733–744, 1988
- [2] H. Hobara, Y. Kobayashi, T. Nakamura, N. Yamasaki, K. Nakazawa, M. Akai, and T. Ogata, "Lower extremity joint kinematics of stair ascent in transfemoral amputees," *Prosthetics and Orthotics International*, vol. 35, no. 4, pp. 467–472, 2011.
- [3] T. S. Bae, K. Choi, D. Hong, and M. Mun, "Dynamic analysis of aboveknee amputee gait," *Clin. Biomech.*, vol. 22, pp. 557–566, 2007.
- [4] R. Gailey, K. Allen, J. Castles, J. Kucharik, and M. Roeder, "Review of secondary physical conditions associated with lower-limb amputation and long-term prosthesis use," *J. Rehabilitation Research and Develop*ment, vol. 45, pp. 15–30, 2008.
- [5] D. J. Lura, M. W. Wernke, S. L. Carey, J. T. Kahle, R. M. Miro, and M. J. Highsmith, "Crossover study of amputee stair ascent and descent biomechanics using Genium and C-Leg prostheses with comparison to non-amputee control," *Gait and Posture*, vol. 58, pp. 103–107, 2017.
- [6] D. M. Ehde, D. G. Smith, J. M. Czerniecki, K. M. Campbell, D. M. Malchow, and L. R. Robinson, "Back pain as a secondary disability in persons with lower limb amputations," *Arch. Phys. Med. Rehabil.*, vol. 82, no. 6, pp. 731–734, 2001.
- [7] D. Norvell, J. Czerniecki, G. Reiber, C. Maynard, J. Pecoraro, and N. Weiss, "The prevalence of knee pain and symptomatic knee osteoarthritis among veteran traumatic amputees and nonamputees," *Arch. Phys. Med. Rehabil.*, vol. 86, no. 3, pp. 487–493, 2005.
- [8] P. A. Struyf, C. M. van Heugten, M. W. Hitters, and R. J. Smeets, "The Prevalence of Osteoarthritis of the Intact Hip and Knee Among Traumatic Leg Amputees," *Arch. Phys. Med. Rehabil.*, vol. 90, no. 3, pp. 440–6, 2009.
- [9] T. Schmalz, S. Blumentritt, and B. Marx, "Biomechanical analysis of stair ambulation in lower limb amputees," *Gait and Posture*, vol. 25, pp. 267–278, 2 2007.
- [10] B. E. Lawson, J. Mitchell, D. Truex, A. Shultz, E. Ledoux, and M. Gold-farb, "A robotic leg prosthesis: Design, control, and implementation," *IEEE Robotics and Automation Magazine*, vol. 21, pp. 70–81, 2014.
- [11] T. Lenzi, M. Cempini, L. Hargrove, and T. Kuiken, "Design, development, and testing of a lightweight hybrid robotic knee prosthesis," *Int. J. Robotics Research*, vol. 37, pp. 953–976, 2018.
- [12] M. Tran, L. Gabert, M. Cempini, and T. Lenzi, "A Lightweight, Efficient Fully Powered Knee Prosthesis with Actively Variable Transmission," *IEEE Robot. Autom.*, vol. 4, no. 2, pp. 1186–1193, 2019.
- [13] T. Elery, S. Rezazadeh, C. Nesler, and R. D. Gregg, "Design and Validation of a Powered Knee-Ankle Prosthesis With High-Torque, Low-Impedance Actuators," *IEEE Trans. Robot.*, pp. 1–20, 2020.
- [14] A. F. Azocar, L. M. Mooney, J. F. Duval, A. M. Simon, L. J. Hargrove, and E. J. Rouse, "Design and clinical implementation of an open-source bionic leg," *Nat. Biomed. Eng.*, vol. 4, no. 10, pp. 941–953, 2020.
- [15] H. L. Bartlett, S. T. King, M. Goldfarb, and B. E. Lawson, "Design and assist-as-needed control of a lightly powered prosthetic knee," *IEEE Trans. Medical Robotics and Bionics*, vol. 4, pp. 490–501, 2022.
- [16] M. Tran, L. Gabert, S. Hood, and T. Lenzi, "A lightweight robotic leg prosthesis replicating the biomechanics of the knee, ankle, and toe joint," *Science Robotics*, vol. 7, no. 72, p. eabo3996, 2022.
- [17] E. J. Wolf, V. Q. Everding, A. L. Linberg, B. L. Schnall, J. M. Czerniecki, and J. M. Gambel, "Assessment of transfemoral amputees using C-Leg and Power Knee for ascending and descending inclines and steps," *J. Rehabil. Res. Dev.*, vol. 49, no. 6, p. 831, 2012.
- [18] J. Camargo, K. Bhakta, K. Herrin, and A. Young, "Biomechanical evaluation of stair ambulation using impedance control on an active prosthesis," *J. biomechanical engineering*, vol. 145, 2 2023.
- [19] F. Sup, H. Varol, J. Mitchell, T. Withrow, and M. Goldfarb, "Self-contained powered knee and ankle prosthesis: Initial evaluation on a transfermoral amputee," *IEEE Int. Conf. Rehabil. Robot.*, pp. 638–644, 2009.
- [20] B. E. Lawson, H. A. Varol, A. Huff, E. Erdemir, and M. Goldfarb, "Control of stair ascent and descent with a powered transfemoral prosthesis," *IEEE Trans. Neural Syst. Rehabilitation Eng.*, vol. 21, no. 3, pp. 466–473, 2013.
- [21] A. M. Simon, K. A. Ingraham, N. P. Fey, S. B. Finucane, R. D. Lipschutz, A. J. Young, and L. J. Hargrove, "Configuring a powered knee and ankle prosthesis for transferoral amputees within five specific ambulation modes," *PLoS ONE*, vol. 9, no. 6, 2014.
- [22] E. D. Ledoux and M. Goldfarb, "Control and evaluation of a powered transfemoral prosthesis for stair ascent," *IEEE Trans. Neural Syst. Rehabilitation Eng.*, vol. 25, no. 7, pp. 917–924, 2017.

- [23] S. Culver, H. Bartlett, A. Shultz, and M. Goldfarb, "A stair ascent and descent controller for a powered ankle prosthesis," *IEEE Trans. Neural* Syst. Rehabilitation Eng., vol. 26, pp. 993–1002, 2018.
- [24] R. Gehlhar, M. Tucker, A. J. Young, and A. D. Ames, "A review of current state-of-the-art control methods for lower-limb powered prostheses," *Annual Reviews in Control*, 2023.
- [25] R. Riener, M. Rabuffetti, and C. Frigo, "Stair ascent and descent at different inclinations," *Gait and Posture*, vol. 15, pp. 32–44, 2002.
- [26] J. Camargo, A. Ramanathan, W. Flanagan, and A. Young, "A comprehensive, open-source dataset of lower limb biomechanics in multiple conditions of stairs, ramps, and level-ground ambulation and transitions," *J. Biomech.*, vol. 119, p. 110320, 2021.
- [27] E. Reznick, K. Embry, R. Neuman, E. Bolívar-Nieto, N. Fey, and R. Gregg, "Human lower-limb kinematics and kinetics during continuously varying locomotion," *Scientific Data*, pp. 1–15, 2021.
- [28] H. Huang, D. L. Crouch, M. Liu, G. S. Sawicki, and D. Wang, "A cyber expert system for auto-tuning powered prosthesis impedance control parameters," Ann. Biomed. Eng., 2016.
- [29] M. Li, Y. Wen, X. Gao, J. Si, and H. Huang, "Toward expedited impedance tuning of a robotic prosthesis for personalized gait assistance by reinforcement learning control," *IEEE Trans. Robotics*, vol. 38, no. 1, pp. 407–420, 2022.
- [30] R. Wu, M. Li, Z. Yao, W. Liu, J. Si, and H. Huang, "Reinforcement learning impedance control of a robotic prosthesis to coordinate with human intact knee motion," *IEEE Robot. Autom.*, vol. 7, no. 3, pp. 7014– 7020, 2022.
- [31] D. Quintero, D. J. Villarreal, D. J. Lambert, S. Kapp, and R. D. Gregg, "Continuous-phase control of a powered knee-ankle prosthesis: Amputee experiments across speeds and inclines," *IEEE Trans. Robotics*, vol. 34, no. 3, pp. 686–701, 2018.
- [32] S. Rezazadeh, D. Quintero, N. Divekar, E. Reznick, L. Gray, and R. D. Gregg, "A phase variable approach for improved rhythmic and non-rhythmic control of a powered knee-ankle prosthesis," *IEEE Access*, vol. 7, pp. 109 840–109 855, 2019.
- [33] T. Elery, S. Rezazadeh, E. Reznick, L. Gray, and R. D. Gregg, "Effects of a Powered Knee-Ankle Prosthesis on Amputee Hip Compensations: A Case Series," *IEEE Trans. Neural Syst. Rehabil. Eng.*, vol. 28, no. 12, pp. 2944–2954, 2020.
- [34] T. K. Best, K. R. Embry, E. J. Rouse, and R. D. Gregg, "Phase-variable control of a powered knee-ankle prosthesis over continuously varying speeds and inclines," in *IEEE/RSJ Int. Conf. Intelligent Robots and* Systems, 2021, pp. 6182–6189.
- [35] R. J. Cortino, E. Bolivar-Nieto, T. K. Best, and R. D. Gregg, "Stair ascent phase-variable control of a powered knee-ankle prosthesis," in *IEEE Int. Conf. Robotics and Automation*, 2022, pp. 5673–5678.
- [36] T. K. Best, C. G. Welker, E. J. Rouse, and R. D. Gregg, "Data-driven variable impedance control of a powered knee-ankle prosthesis for adaptive speed and incline walking," *IEEE Trans. Robotics*, pp. 1–19, 2023.
- [37] C. G. Welker, T. K. Best, and R. D. Gregg, "Data-driven variable impedance control of a powered knee-ankle prosthesis for sit, stand, and walk with minimal tuning," in *IEEE/RSJ Int. Conf. Intelligent Robots* and Systems, 2022, pp. 9660–9667.
- [38] C. D. Hoover, G. D. Fulk, and K. B. Fite, "Stair ascent with a powered transfemoral prosthesis under direct myoelectric control," *IEEE/ASME Trans. Mechatronics*, vol. 18, no. 3, pp. 1191–1200, 2013.
- [39] S. Hood, L. Gabert, and T. Lenzi, "Powered knee and ankle prosthesis with adaptive control enables climbing stairs with different stair heights, cadences, and gait patterns," *IEEE Trans. Robotics*, vol. 38, no. 3, pp. 1430–1441, 2022.
- [40] "504 Stairways ADA Compliance," 2023. [Online]. Available: https://www.ada-compliance.com/ada-compliance/504-stairways
- [41] J. Fernando, "Moving average (ma): Purpose, uses, formula, and examples," 2023. [Online]. Available: https://www.investopedia.com/ terms/m/movingaverage.asp
- [42] N. Aghasadeghi, H. Zhao, L. J. Hargrove, A. D. Ames, E. J. Perreault, and T. Bretl, "Learning impedance controller parameters for lower-limb prostheses," *IEEE Int. Conf. Intelligent Robots and Systems*, pp. 4268– 4274, 2013.
- [43] S. B. Finucane, L. J. Hargrove, and A. M. Simon, "Functional mobility training with a powered knee and ankle prosthesis," *Frontiers in Reha*bilitation Sciences, vol. 3, 4 2022.
- [44] T. K. Best, C. A. Laubscher, R. J. Cortino, S. Cheng, and R. D. Gregg, "Improving amputee endurance over activities of daily living with a robotic knee-ankle prosthesis: A case study," in *IEEE/RSJ Int. Conf. Intelligent Robots and Systems*, 2023.

- [45] E. Reznick, C. G. Welker, and R. D. Gregg, "Predicting individualized joint kinematics over continuous variations of walking, running, and stair climbing," *IEEE Open J. Eng. Med. Biol.*, vol. 3, pp. 211–217, 2022.
- climbing," *IEEE Open J. Eng. Med. Biol.*, vol. 3, pp. 211–217, 2022.

 [46] E. Reznick, K. Embry, and R. D. Gregg, "Predicting individualized joint kinematics over a continuous range of slopes and speeds," in *IEEE Int. Conf. Biomedical Robotics and Biomechatronics*, 2020, pp. 666–672.
- [47] E. Reznick, "Understanding individuality in human locomotion for configuring powered prosthetic legs," PhD thesis, University of Michigan, August 2023.

1

Data-Drive Phase-Based Control of a Powered Knee-Ankle Prosthesis for Variable-Incline Stair Ascent and Descent: Supplementary Material

Ross J. Cortino, T. Kevin Best, and Robert D. Gregg

CONTENTS

I	Hybrid Kinematic-Impedance Controller (HKIC) Supplements					
	I-A	State Transition Criteria for Unified Phase Variable Definition	2			
	I-B	Impedance Parameter Optimization Constraints	2			
	I-C	Stair Descent Impedance Model	2			
II	Experiment Supplements					
	II-A	Participant Information	3			
	II-B	Kinematic Comparison Tables Across Step Heights	3			
	II-C	Kinetic Comparison Tables Across Step Heights	5			

I. HYBRID KINEMATIC-IMPEDANCE CONTROLLER (HKIC) SUPPLEMENTS

A. State Transition Criteria for Unified Phase Variable Definition

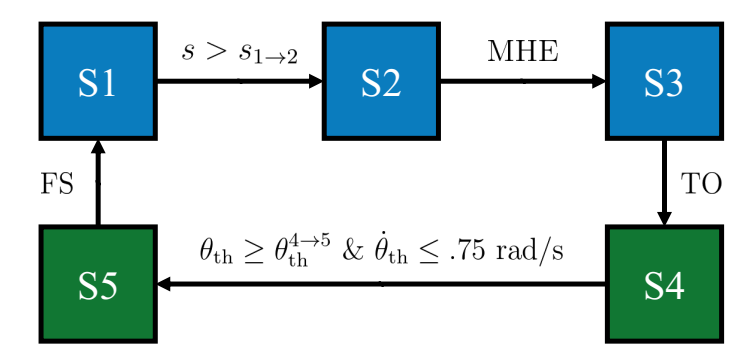


Fig. 1. A visual representation of the state machine that governs the unified phase variable for stair ascent and descent. The blue squares correspond to the stance phase variable definition, while the green squares correspond to the swing phase variable definition. Refer to the main text for parameter definitions.

B. Impedance Parameter Optimization Constraints

TABLE I
IMPEDANCE PARAMETER OPTIMIZATION CONSTRAINTS

Constraint	Ascent		Descent	
	Ankle	Knee	<u>Ankle</u>	Knee
min FS Stiffness Nm/kg	3.5	1.5	3.0	1.0
min Stiffness Nm/kg rad	3.5	1.0	1.0	0.5
min Damping Nms/kg rad	0.01	0.01	0.01	0.01
max Damping Nms/kg	0.14	0.14	0.14	0.14

C. Stair Descent Impedance Model

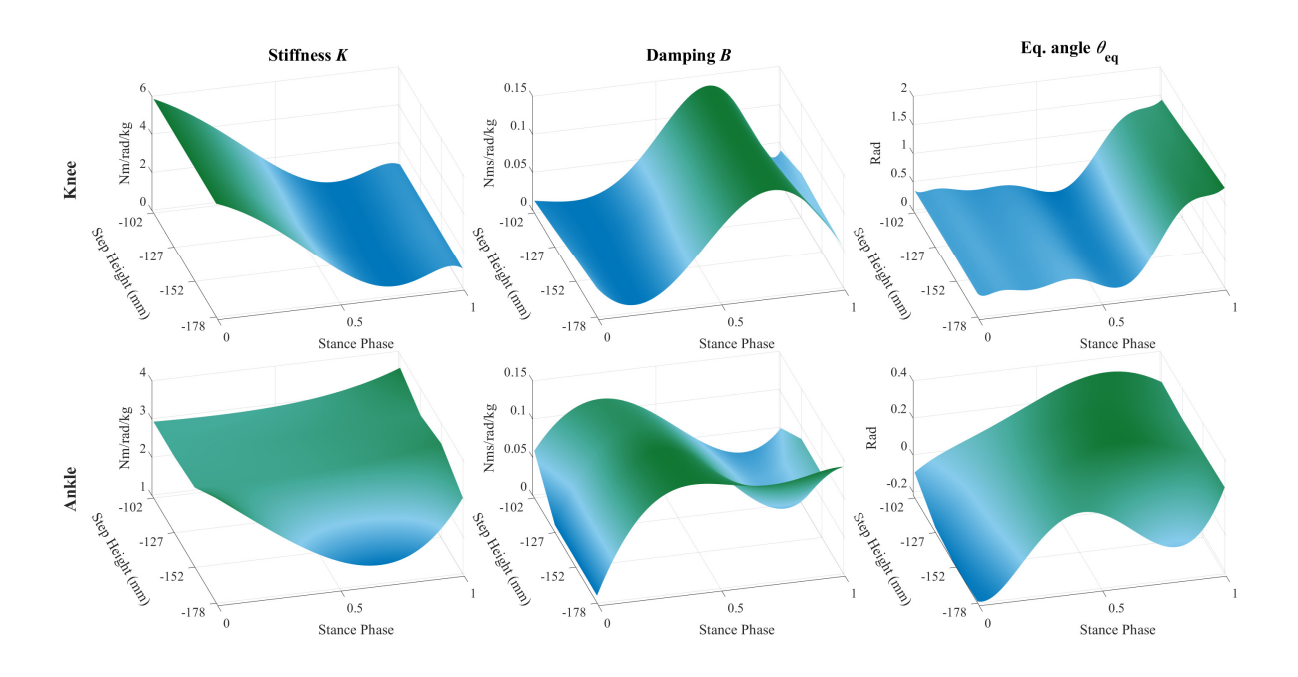


Fig. 2. Plots of the calculated stair descent impedance functions for stiffness $K(s_{\rm st},\gamma)$, damping $B(s_{\rm st},\gamma)$, and equilibrium angle $\theta_{\rm eq}(s_{\rm st},\gamma)$ for the knee and ankle over the range of step height configurations from $\pm (102 \text{ to } 178) \text{ mm}$.

II. EXPERIMENT SUPPLEMENTS

A. Participant Information

TABLE II PARTICIPANT ATTRIBUTES

ID	Sex	Age (yrs)	Mass (kg)	Height (m)	Years since amputation	Etiology
P1	Male	26	116	1.9	26	Congenital
P2	Male	18	76	1.8	18	Congenital

B. Kinematic Comparison Tables Across Step Heights

 $\begin{tabular}{ll} \textbf{TABLE III} \\ \textbf{ASCENT KINEMATIC COMPARISONS ACROSS STAIR CONFIGURATIONS}^1 \\ \end{tabular}$

Metric	Step Height (mm)	AB	P1 HKIC	P2 HKIC	P2 PAS
Max	102	88.81±5.04	85.67±1.21	81.79±5.86	111.66±8.38
Knee	127	91.45±4.91	87.86±1.34	83.85±3.05	117.82±4.57
Angle (°)	152	96.31±5.4	94.13±0.85	93.58±1.41	122.39±2.49
	178	100.34±6.28	99.52±2.91	-	125.57±1.01
Min	102	15.14±4.42	19.21±1.05	11.67±1.62	2.74±0.42
Knee	127	16.81±4.69	14.96±2.34	12.83±1.96	2.99 ± 0.41
Angle (°)	152	17.85±5.74	18.43±1.42	12.50±2.09	3.53±0.38
	178	17.87±4.73	15.9±2.35	-	3.74±0.49
Foot-	102	56.72±3.95	56.98±1.04	56.83±4.78	53.58±2.60
Strike Knee	127	62.46±4.36	65.03±2.36	61.07±2.81	55.95±1.99
Angle	152	68.86±4.33	69.42±1.81	69.21±4.01	59.93±3.77
(°)	178	74.03±4.18	77.93±1.21	-	57.18±2.42
Ankle	102	21.91±3.22	21.77±0.51	23.10±1.04	10.61 ± 0.82
Dorsi- flexion	127	23.71±3.21	23.91±0.42	24.19±1.58	10.69 ± 0.90
Angle	152	25.42±4.01	24.04±0.63	26.87±3.05	11.57±1.79
(°)	178	26.70±5.34	27.19±0.63	-	8.22±1.08
Ankle Plan-	102	1.94±5.13	-0.46±0.73	1.27±0.58	4.35±0.41
tarflex-	127	-1.06±5.14	-3.07±0.24	-1.76±0.33	4.55±0.53
ion Angle	152	-4.35±7.12	-7.6±0.97	-5.83±0.85	5.78 ± 0.32
(°)	178	-7.13±7.70	-10.49±1.05	-	$3.93{\pm}0.32$
Foot-	102	18.53±3.44	19.37±0.6	19.81±3.01	6.68±0.36
Strike Ankle	127	20.02±3.68	21.53±0.87	21.19±2.70	6.81±0.53
Angle	152	21.81±5.11	23.35±0.55	25.57±4.22	7.74±0.61
(°)	178	22.87±6.14	25.78±0.51	-	6.51±0.56

¹Bolded entries indicate results within a standard deviation of the AB reference.

 $\label{total loss} \textbf{TABLE IV} \\ \textbf{Descent Kinematic Comparisons Across Stair Configurations}^2$

Measure	Step Height (mm)	AB	P1 HKIC	P2 HKIC	P2 PAS
Max	102	85.26±4.95	79.36±3.5	75.15±0.87	72.92±2.94
Knee	127	90.15±7.11	85.22±3.77	82.32±2.01	78.87±2.49
Angle (°)	152	95.01±7.76	91.38±2.32	88.40±2.39	84.04±2.29
	178	100.43±5.28	95.13±2.68	-	88.98±3.01
Min	102	18.44±5.13	15.63±1.84	15.88±0.81	11.48±0.39
Knee	127	19.19±5.63	17.19±2.6	15.87±3.00	11.57±0.49
Angle	152	19.62±5.99	16.56±3.43	15.97±3.37	12.29±0.44
(°)	178	19.11±4.19	13.31±3.54	-	12.38±0.53
Foot-	102	19.41±4.94	20.36±0.47	16.69±1.35	11.94±0.54
Strike Knee	127	19.83±5.70	20.75±0.95	17.51±4.54	12.20±0.5
Angle	152	19.96±6.40	20.38±0.66	17.06±3.69	13.01±0.37
(°)	178	19.85±3.72	20.7±0.69	-	13.47±0.53
Ankle	102	37.04±3.84	30.51±0.62	30.85±2.03	6.93±2.12
Dorsi- flexion	127	37.38±6.57	31.82±0.75	33.92±0.69	7.84±1.72
Angle	152	37.86±6.68	30.75±0.91	36.63±0.49	9.31±1.31
(°)	178	38.73±5.53	32.64±2.09	-	8.19±1.61
Ankle Plan-	102	-15.50±5.32	-15.9±0.72	-15.33±0.09	3.21±0.34
tarflex-	127	-17.51±7.34	-17.57±0.58	-16.66±0.47	3.75±0.25
ion Angle	152	-19.33±8.39	-20.17±0.76	-18.15±1.48	4.75±0.33
(°)	178	-22.09±5.10	-23.25±0.68	-	3.72±0.23
Foot-	102	-5.95±5.08	-5.28±0.88	-2.76±1.18	3.99±0.17
Strike Ankle	127	-8.30±7.53	-8.37±0.58	-4.78±4.62	4.14±0.14
Angle	152	-10.43±8.18	-10.08±0.57	-7.48±5.07	4.85±0.36
(°)	178	-12.31±5.53	-11.84±0.67	-	3.88±0.13

 $^{^2\}mbox{Bolded}$ entries indicate results within a standard deviation of the AB reference.

C. Kinetic Comparison Tables Across Step Heights

Measure	Step Height (mm)	AB	P1 HKIC	P2 HKIC
Peak	102	-0.74±0.30	-0.84±0.08	-0.81±0.08
Knee	127	-0.88±0.29	-1.12±0.11	-0.95±0.06
Torque (Nm/kg)	152	-1.04±0.31	-1.22±0.06	-1.21±0.07
(INIII/Kg)	178	-1.13±0.34	-1.44±0.04	-
	102	0.34±0.14	0.33±0.03	0.32±0.05
Knee Work	127	0.38 ± 0.14	0.52±0.07	0.47±0.03
(J/kg)	152	0.51±0.18	$0.61{\pm}0.05$	0.58±0.07
	178	0.59 ± 0.21	0.82±0.06	-
Peak	102	-1.34±0.24	-1.03±0.03	-0.72±0.14
Ankle	127	-1.36±0.26	-0.95±0.06	-0.86±0.06
Torque (Nm/kg)	152	-1.41±0.26	-1.02±0.05	-0.96±0.08
(IVIII/Kg)	178	-1.39±0.26	-0.98±0.07	-
	102	0.22±0.1	0.15±0.01	0.06±0.02
Ankle Work	127	0.30 ± 0.13	0.17±0.02	0.07±0.03
(J/kg)	152	0.37±0.14	0.24±0.02	0.14±0.06
	178	0.46 ± 0.15	0.34±0.02	-

³Bolded entries indicate results within a standard deviation of the AB reference or match and/or exceed AB Normative performance.

 $\begin{array}{c} \text{TABLE VI} \\ \text{Descent Knee and Ankle Kinetics}^4 \end{array}$

Measure	Step Height (mm)	AB	P1 HKIC	P2 HKIC
Peak	102	-0.98±0.24	-0.83±0.06	-0.77±0.05
Knee	127	-1.03±0.24	-1.25±0.21	-0.78±0.07
Torque (Nm/kg)	152	-1.12±0.27	-1.05±0.27	-0.94±0.06
(NIII/Kg)	178	-1.20±0.28	-1.07 ± 0.14	-
	102	-0.65±0.15	-0.34±0.07	-0.15±0.04
Knee Work	127	-0.8±0.19	-0.53±0.13	-0.25±0.04
(J/kg)	152	-0.89±0.18	-0.56±0.15	-0.33±0.03
	178	-1.04±0.21	-0.59±0.12	-
Peak	102	-0.96±0.24	-0.76±0.04	-0.81±0.08
Ankle	127	-1.01±0.23	-0.98±0.12	-0.99±0.08
Torque (Nm/kg)	152	-1.01±0.36	-0.84±0.11	-1.06±0.05
(Mill/kg)	178	-1.07±0.26	-0.92±0.06	-
	102	-0.26±0.13	-0.22±0.01	-0.27±0.03
Ankle Work	127	-0.35±0.13	-0.35±0.03	-0.37±0.03
(J/kg)	152	-0.44±0.15	-0.3±0.06	-0.39±0.06
	178	-0.51±0.15	-0.27±0.02	-

⁴Bolded entries indicate results within a standard deviation of the AB reference.